Chemical Science

ROYAL SOCIETY OF CHEMISTRY

REVIEW

View Article Online
View Journal | View Issue

Cite this: *Chem. Sci.*, 2025, **16**, 20662

Reconstruction chemistry of electrocatalysts under working conditions

Hui Chen, Lina Wang, Muhan Na and Xiaoxin Zou *

Reconstruction is a common phenomenon in electrocatalytic processes, playing a critical role in determining catalytic activity and stability. With growing fundamental understanding of reconstruction chemistry, the deliberate regulation of reconstruction has emerged as a pivotal strategy for designing ideal electrocatalysts. In this review, we first outline diverse reconstruction processes observed in key catalytic reactions, such as the oxygen evolution reaction and CO_2 reduction reaction. We then summarize the external (*e.g.*, potential, electrolyte, and temperature) and internal factors (*e.g.*, composition, crystal structure, and crystallinity) that govern reconstruction dynamics and subsequent catalytic behavior. Based on these insights, we discuss general approaches to modulate reconstruction, including pre-catalyst design and electrolyte engineering. Furthermore, we highlight advanced *in situ*/*operando* characterization techniques that are indispensable for probing reconstruction mechanisms at atomic and electronic levels. Finally, we propose future research directions, emphasizing the need for mechanistic studies coupling multiple characterization techniques with theoretical modelling, as well as the development of reconstruction-resistant or reconstruction-optimized electrocatalysts tailored for industrial applications. This review aims to provide a comprehensive framework for understanding and harnessing reconstruction chemistry to design highly efficient and stable electrocatalysts.

Received 28th August 2025
Accepted 16th October 2025

DOI: 10.1039/d5sc06605k

rsc.li/chemical-science

1. Introduction

Electrocatalysis plays a pivotal role in modern sustainable energy systems,[1–4] facilitating critical reactions (Fig. 1a) such as the oxygen evolution reaction (OER), hydrogen evolution reaction (HER), carbon dioxide reduction reaction (CO_2RR), urea oxidation reaction (UOR), and nitrate reduction reaction (NO_3RR). These processes enable the conversion of abundant small molecules (H_2O and CO_2) or environmental pollutants (NO_x) into valuable chemical feedstocks or benign substances through renewable electricity, offering potential benefits for energy storage and environmental remediation. The efficiency of such transformations is intrinsically determined by the performance of electrocatalysts. The ideal electrocatalyst should not only achieve excellent catalytic metrics, including high activity, durability, and product selectivity, but also minimize or completely avoid the use of scarce and expensive noble metals such as Pt, Ir, and Ru.[5,6] Consequently, the development of efficient, sustainable, and cost-effective catalytic materials has become a central research focus. Over the past two decades, a diverse range of catalysts, spanning metals and alloys,[7–9] metal oxides (*e.g.*, perovskite and spinel-type oxides),[10,11] non-oxide compounds (*e.g.*, sulfides and nitrides),[12,13] and carbon-based materials,[14,15] has been intensively explored for driving the electrochemical reactions associated with the water, carbon, and nitrogen cycles.

Chemical reconstruction of electrocatalysts is a prevalent phenomenon in the aforementioned processes, referring to the dynamic rearrangement of atoms in the catalyst under electrochemical conditions. Such structural evolutions are predominantly driven by the applied potential and/or interfacial interactions between the catalyst and reaction species, including reactants, intermediates, products, and electrolyte ions. Typically, reconstruction begins with localized surface modifications, for instance, the oxidation of $Ni(OH)_2$ to NiOOH during the OER,[16,17] and can propagate into bulk-phase transformations over extended operation, such as the complete conversion of Bi_2O_3 into metallic Bi during the CO_2RR.[18,19] The pathway and extent of reconstruction depend on multiple factors (Fig. 1b), such as applied potential, electrolyte, and the initial state of the catalyst. The reconstructed species formed during electrocatalysis serve as the true active phases, whereas their pristine counterparts act merely as precatalysts that undergo *in situ* activation under operational conditions. The majority of reconstructions result in irreversible structural transformations (Fig. 1c). In certain situations, surface reconstruction can be reversible, meaning that the surface recovers its initial state once external factors such as potential is removed.[20,21] Since these transient structural variations cannot be captured by *ex situ* techniques, it is essential to investigate the electrocatalyst surface directly under *in situ* conditions.

State Key Laboratory of Inorganic Synthesis and Preparative Chemistry, College of Chemistry, Jilin University, 2699 Qianjin Street, Changchun 130012, China. E-mail: xxzou@jlu.eu.cn

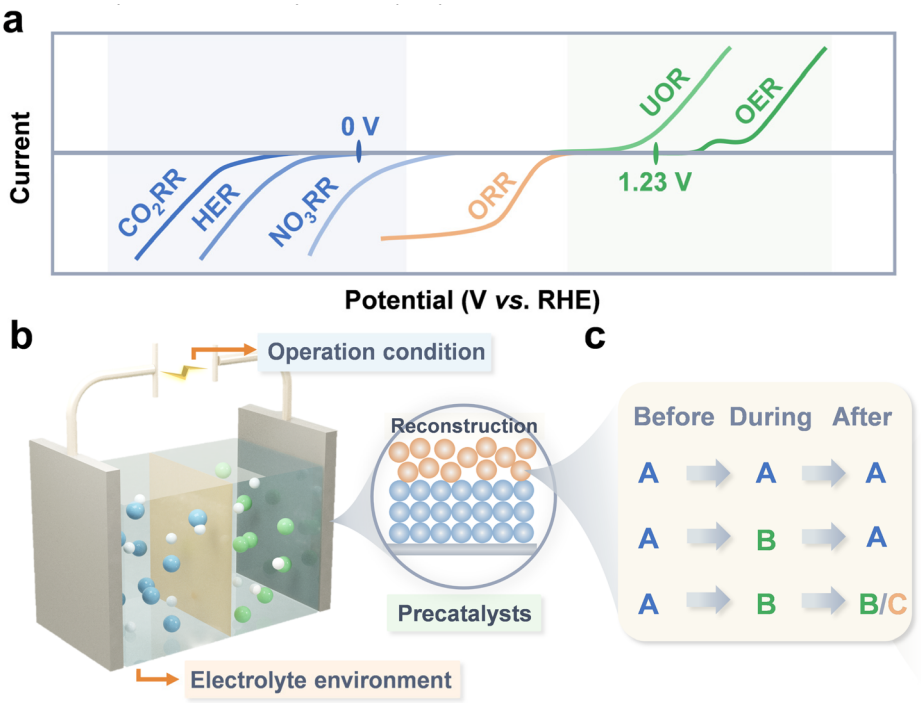

Fig. 1 (a) Typical electrocatalytic reactions exhibiting reconstruction phenomena and their corresponding polarization curves. (b) Key factors governing the reconstruction process, including reaction conditions, electrolyte environment, and initial state of catalyst. (c) Schematic illustration of electrocatalysts undergoing no reconstruction, reversible reconstruction, and irreversible reconstruction.

Reconstruction plays a critical role in determining both the activity and stability of electrocatalysts. During this dynamic process, the fundamental properties of the catalyst, including its crystalline phase, chemical composition, crystallinity and electronic structure, may undergo substantial transformations. These structural evolutions can have dual effects on catalytic performance: while some reconstructions enhance activity by creating favourable active sites,[22–24] others may degrade performance through active site poisoning or dissolution.[25,26] The stability of electrocatalysts is equally susceptible to reconstruction effects. Beneficial reconstructions can establish robust active configurations that maintain long-term operation, whereas detrimental transformations may lead to rapid deactivation through mechanisms such as active site destruction or material degradation.[27] This delicate balance between performance enhancement and deterioration underscores the importance of understanding and controlling reconstruction processes in electrocatalyst design.

Understanding the reconstruction process remains a significant challenge, as it often demands the integration of multiple *in situ* characterization techniques. Traditional *ex situ* methods, such as microscopic and spectroscopic analyses, can elucidate the structural and chemical states of catalysts before and after reconstruction, yet they are inherently incapable of capturing the real-time, dynamic evolution of catalysts under operating conditions, particularly in the case of reversible transformations. To overcome this limitation, researchers have increasingly focused on developing *in situ*/*operando* characterization techniques, which enable real-time monitoring of reconstruction dynamics, identification of true active phases, and detection of transient intermediates.[28–31] Recent advances in these methodologies have significantly deepened our understanding of reconstruction chemistry, providing critical insights for controlling and tailoring the process.[32,33] As a result, deliberate modulation of reconstruction has emerged as a powerful approach for designing high-performance electrocatalysts.

In this review, we systematically examine the complex landscape of electrocatalyst reconstruction under operational conditions. We begin by categorizing various reconstruction phenomena observed across important electrochemical reactions (OER, CO_2RR, *etc.*) and analysing the fundamental mechanisms governing these transformations. Building on these foundational insights, we discuss innovative strategies for precisely controlling reconstruction processes through precatalyst design and reaction microenvironment engineering. Special attention is given to how these approaches can be leveraged to enhance both activity and stability of electrocatalysts. The review then provides a critical assessment of advanced *in situ*/*operando* characterization techniques that have revolutionized our ability to probe reconstruction dynamics at atomic scales. Finally, we identify key challenges and future opportunities in reconstruction chemistry, particularly emphasizing the need for combining multiple characterization techniques with computational modelling, as well as developing design principles for reconstruction-aware catalysts for practical application.

2. Typical reconstruction types

The reconstruction of electrocatalysts is fundamentally governed by the thermodynamic drive to minimize free energy. Applied potentials modify the electrochemical potential, thereby triggering atomic rearrangements, while adsorbed reaction intermediates and electrolyte species further regulate surface energetics. Depending on the specific reconstruction pathway, the resulting structural variations may involve electrochemical oxidation and reduction, dissolution and redeposition, phase transition, as well as surface adsorption and coordination (Fig. 2). Notably, these processes are not mutually exclusive and can occur simultaneously, often coupling with one another to shape the dynamic evolution of the catalyst structure.

2.1 Electrochemical oxidation and reduction

During anodic oxidation reactions such as the OER and UOR, most metal-based catalysts inevitably undergo changes in metal valence states (Fig. 2a).[34–36] Under typical operating conditions, surface metal atoms are oxidized, either reversibly or irreversibly, into higher valence states, with the transition extent dictated by the applied potential and reaction duration. This behavior arises because the oxidation potentials of catalytically active transition metals (typically 1.0–1.5 V *vs.* RHE) coincide with the potential range required for the OER and UOR.[37] For example, Ni-, Co-, and Fe-based catalysts are readily transformed into high-valence oxides or hydroxides such as NiOOH, CoOOH, and FeOOH.[38–41] In some cases, excessive oxidation can yield insoluble species, for instance, the formation of RuO_4^{2-} from Ru-based catalysts, ultimately causing structural degradation.[42]

In cathodic reduction reactions including the HER and CO_2RR, metal-based catalysts typically undergo reductive reconstruction to metals.[43,44] During these processes, metal oxides, hydroxides, and non-oxide compounds (including chalcogenides, nitrides, and phosphides) are commonly reduced to their metallic states (*e.g.*, Cu, Bi, Zn, and In).[45–48] This transformation is accompanied by the extraction and migration of anions (*e.g.*, O, Se, N, and P), leading to substantial changes in the catalyst's morphology, composition, and shape.[49–51] Notably, these reconstructions often generate new interfaces and various defects, including atomic steps, lattice distortions, vacancies, and cavities, which can significantly influence catalytic performance.[52,53] However, complete reduction to metallic states is not always achieved. In many cases, partial reduction occurs, resulting in mixed-phase catalysts containing both metallic and oxidized components. An example is the evolution of Cu_2O catalysts into Cu/Cu_2O heterostructures during the CO_2RR.[54,55]

2.2 Dissolution and redeposition

Metal dissolution in electrocatalysts during electrochemical operation is typically driven by a combination of factors (Fig. 2b), including the intrinsic thermodynamic instability of certain metals in acidic or alkaline electrolytes, their over-oxidation into soluble high-valence species, and involvement of lattice oxygen mechanism (LOM). The leaching of metal cations not only alters the elemental composition but can also induce crystal structure distortion and changes in metal valence states. For chemically unstable elements, dissolution may occur even at open-circuit potential. For example, Fe-, Co-, and Ni-based oxides, exhibit high activity for the OER in neutral or alkaline media but suffer severe corrosion in acidic environments.[56] The leaching of such structural components often leads to lattice destabilization and eventual collapse. Even thermodynamically stable metals under open-circuit conditions can dissolve during the OER, as high anodic potentials promote their oxidation to

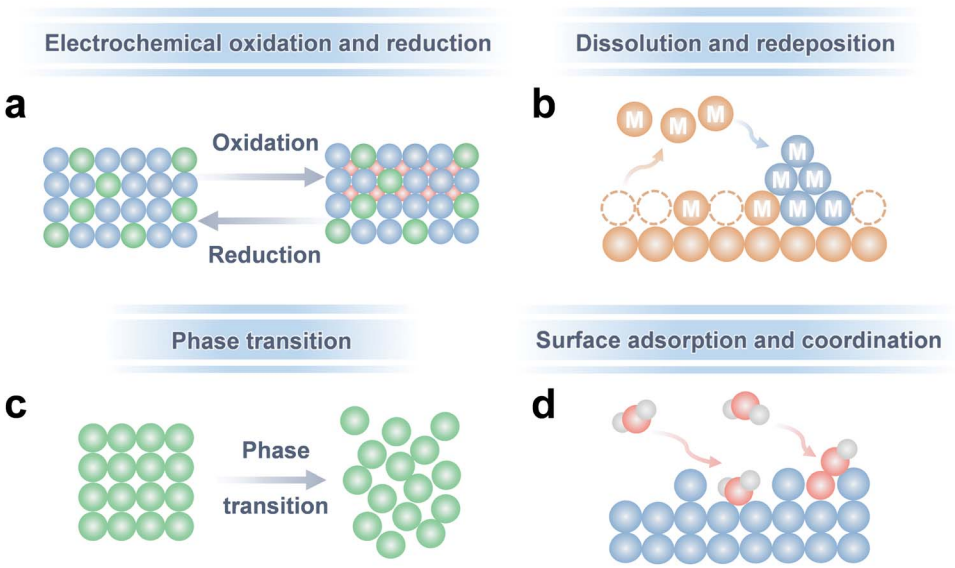

Fig. 2 Typical reconstruction types of electrocatalysts under working conditions, including (a) electrochemical oxidation and reduction, (b) dissolution and redeposition, (c) phase transition, and (d) surface adsorption and coordination.

soluble high-valence species. A RuO_2 catalyst serves as a representative case, undergoing overoxidation–dissolution under OER conditions.[57]

The dissolution process is not confined to metal cations but can also involve anionic species, particularly in metal chalcogenides, nitrides, and phosphides used as OER catalysts. Anions such as B and S may react with the electrolyte to form soluble complexes (*e.g.*, BO_2^- and PO_4^{3-}).[58–60] In some cases, a fraction of these anions remains within the solid catalysts, leading to the formation of core–shell structures, as exemplified by NiSe/NiO_x and Ni_2P/NiO_x.[61,62] During surface reconstruction, especially in poorly crystalline oxides or hydroxides, lattice oxygen can be released *via* the LOM, escaping as molecular O_2.[63,64] Such anion dissolution processes frequently exhibit synergistic effects with cation leaching, thereby accelerating structural degradation and performance loss.

The phenomenon of dissolution–redeposition has been widely observed in various metal-based catalysts, including Mn, Fe, Ni, and Ir,[65–68] indicating a dynamic equilibrium between catalyst dissolution and reprecipitation during electrocatalysis. Recent investigations have elucidated the critical role of this process in determining catalytic performance. For instance, in the acidic OER, Sr_2FeIrO_6 perovskites exhibit Ir leaching followed by redeposition, with this dynamic equilibrium directly governing the ultimate OER activity.[69] Similarly, studies on Zn-doped Cu_2O nano-octahedra under CO_2RR conditions have demonstrated continuous Zn leaching and redeposition,[70] resulting in a dynamic surface stability that sustains catalytic performance.

2.3 Phase transition

During oxidation–reduction and dissolution–redeposition processes, phase transitions are inevitably involved (Fig. 2c). These transitions can occur either within the bulk or at the surface of pristine catalysts. Under electrochemical oxidation conditions, pristine catalysts often transform into amorphous or poorly crystalline hydrated materials or oxyhydroxides. Such poorly crystalline oxyhydroxides may consist of multiple complex phases (*e.g.*, α-, β-, and γ-NiOOH). For example, recent studies have revealed that NiFe and CoFe layered double hydroxides (LDHs) convert from their as-synthesized α-phase to an activated γ-phase during the OER.[71] Similarly, (NiFe)$(OH)_2$ preferentially transforms into γ-(NiFe)OOH under OER conditions. When the applied potential is removed, γ-(NiFe)OOH spontaneously reverts to (NiFe)$(OH)_2$,[58] a process that represents reversible reconstruction. In contrast, under reductive conditions, the metallic state is generally more stable, and reaction intermediates may diffuse into the metal lattice to form unique crystalline phases. A representative example is the electrochemical hydrogen intercalation into Pd during the HER and CO_2RR, leading to the *in situ* formation of PdH_x.[72,73]

Reconstruction-induced phase transitions can generate metastable crystalline phases or facets that are difficult to obtain through conventional chemical synthesis. For example, during the OER process, cation leaching from iridate structures is frequently observed as a result of acid and/or oxidative corrosion.[74–76] The resulting iridate-derived amorphous IrO_x phases may incorporate metastable motifs such as anatase IrO_2, IrO_3, or honeycomb-like IrO_xH_y.[77–79] In addition, open-framework iridates have been reported to reconstruct into rutile nanocrystals with a preferential exposure of the high-index (200) facet,[80] rather than forming the more common low-crystallinity IrO_x species.

2.4 Surface adsorption and coordination

Surface functional groups may coordinate with specific atomic sites of the catalyst to form surface coordination compounds (Fig. 2d). These groups typically originate from three primary sources: (i) reaction intermediates. For example, in the NO_3RR, the NO_2^- intermediate can accumulate on the catalyst surface.[81] (ii) Ions generated from catalyst dissolution. During the OER catalyzed by NiSn@triMPO_4, P release can lead to the formation of PO_4^{3-}, which subsequently adsorbs on Ni sites.[59] (iii) Ions from the electrolyte. For example, in OER electrocatalysis using NiFe foam, thiourea present in the electrolyte can be oxidized to SO_4^{2-}, which then adsorbs on the catalyst surface.[82]

3. Role of reconstruction in electrocatalysis

In situ reconstruction exerts a complex influence on electrochemical performance, which invariably results in either improvement or degradation of catalytic activity. Moreover, the reconstruction pathway is governed by multiple factors, including both external factors (*e.g.*, potential, reaction temperature, and pH) and internal factors (*e.g.*, crystal structure and crystallinity of precatalysts).

3.1 Impact of reconstruction on performance

In situ reconstruction continues to attract significant research interest, primarily because the reconstructed catalysts often exhibit superior apparent activity compared to their directly synthesized counterparts. The enhanced catalytic performance may originate from two main factors.

On the one hand, the structural reconstruction can induce morphological changes, such as surface roughening, leading to increased electrochemical active surface area (Fig. 3a). For instance, in $AIrO_3$-type oxides (A = Sr or Ba) used for acidic OER,[83] Chung *et al.* demonstrated that alkaline-earth leaching could result in a more than 20-fold increase in active surface area.

On the other hand, the reconstructed phases often demonstrate superior intrinsic activity due to their unique structural characteristics, including defect-rich surfaces, unsaturated coordination sites, unique surface decorations, and metastable states (Fig. 3b). These features are typically unattainable through conventional synthesis methods. For example, our group demonstrated that metal borides undergo *in situ* formation of surface-oxidized layers containing stable boron species under OER conditions.[84] The presence of metaborate species induces electron redistribution within the surface oxyhydroxide layers, leading to exceptional catalytic performance. Similarly,

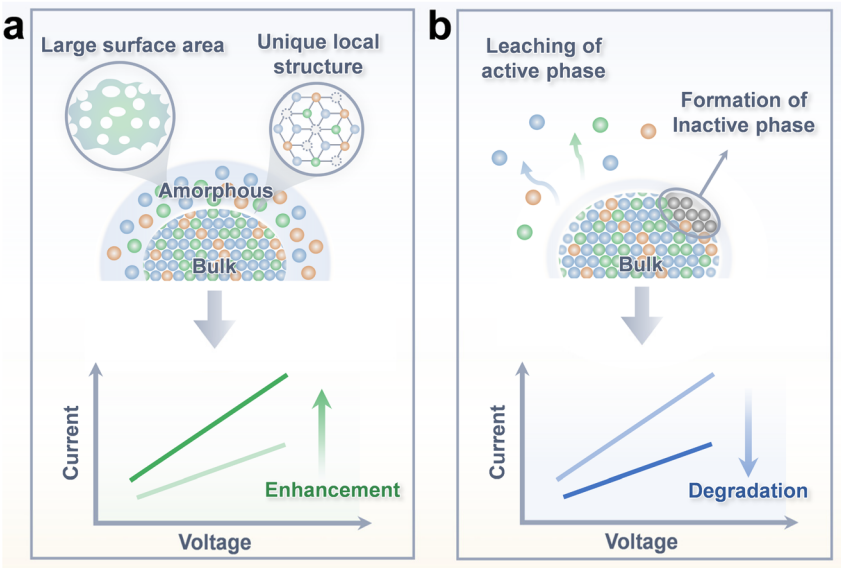

Fig. 3 (a) Schematic representation of the reconstructed surface featuring a large surface area and unique local structure, both of which are conducive to improved catalytic performance. (b) Illustration of the mechanism underlying catalyst degradation during electrocatalysis, highlighting the leaching of active elements and formation of inactive phases, which result in decreased activity.

Lou *et al.* reported that iron cobalt (oxy)phosphide (Fe–Co–P) catalysts largely transform into oxide (Fe–Co–P–O) during OER operation,[85] where the resulting O/P bridges facilitate charge transfer, thereby significantly boosting catalytic activity.

However, structural reconstruction does not always benefit catalysis. In some cases, it may lead to the poisoning of catalytic species, ultimately impairing electrocatalytic performance. A representative example is the catalyst deactivation observed during the CO_2RR, where in situ-formed carbonaceous species poison the catalyst. Recent studies employing *in situ* spectroscopic techniques and trace analysis have demonstrated that carbon deposition and subsequent coverage on polycrystalline Cu foil directly contribute to catalyst deactivation.[86] Electrochemically deposited carbon forms a thin film encapsulating catalyst particles, exhibiting a structure and composition similar to amorphous carbon. This carbon layer exhibits poor electrical conductivity and mass transport properties, severely hindering the diffusion of reactive gases and intermediates during the CO_2RR. The degradation of an initially active phase and the formation of reconstructed structures that lack intrinsic activity represent another detrimental reconstruction pathway. For instance, in Pd–B catalysts,[87] the boron species is crucial for modulating the electronic structure of Pd, enabling high catalytic activity for the HER. However, the leaching of B during catalysis leads to a continuous decline in activity. A similar phenomenon is observed in CuFe alloy electrocatalysts during the CO_2RR,[88] where phase segregation under reducing conditions results in increased hydrogen evolution instead of the desired carbonaceous products.

The impact of structural reconstruction on catalytic stability is primarily determined by the nature of the resulting active phase. A catalyst may undergo dynamic structural changes during operation, but stability is ultimately contingent upon whether these changes yield a robust active phase. For instance, single-atom catalysts, such as Ir–$CoMn_2O_4$,[89] are often structurally dynamic. However, they can reconstruct into specific and stable configurations (*e.g.*, IrO_x/γ-MnO_2) during the OER, which exhibit excellent durability. In addition, different reconstruction pathways can lead to vastly different stability outcomes. While iridates or Ir nanocrystals commonly evolve into amorphous IrO_x phases with poor stability, recent studies have demonstrated that reconstructions can be guided to form highly stable crystalline IrO_2.[80,90] Examples include the transformation of γ-$SrIrO_3$ or Ir/TiO_x@Ti, which achieve remarkable operational stability.

3.2 Factors affecting reconstruction

Reconstruction typically exhibits a time-dependent evolution: a rapid structural transformation during the initial activation phase, followed by a near-steady state in the subsequent stable operation period. The reconstruction process is governed by both external and internal factors (Fig. 1b). Generally, external conditions such as applied voltage, pH, and temperature can affect the reconstruction rate and degree, while intrinsic material properties may determine whether reconstruction occurs and dictate its pathway.

(i) Applied potential: according to the Pourbaix diagram, the applied potential is a critical factor in determining the thermodynamic stability of chemical species during electrocatalysis. For instance, in the electrochemical CO_2RR, a SnO_2 catalyst partially converts into SnO_x species at −0.25 V (*vs.* Ag/AgCl), delivering high faradaic efficiency for formate production.[91] However, when the potential shifts to more negative values (*e.g.*, −1.55 V *vs.* Ag/AgCl), the oxide is reduced to metallic Sn, resulting in much lower selectivity for formate formation. For electrochemical oxidation reactions (*e.g.*, OER), different

metals exhibit distinct potential windows for oxidation and dissolution. For instance, Nakamura *et al.* demonstrated that γ-MnO_2 remains stable only below 1.76 V under acidic OER conditions, above which soluble MnO_4^- species begin to form.[92]

(ii) Electrolyte environment: harsh electrolyte conditions, such as strong acid, strong base and high temperature, often intensify the degree of catalyst reconstruction. For example, Wang *et al.* synthesized an amorphous CoO_xH_y catalyst and investigated its structural evolution during the OER under different pH conditions.[93] Under neutral conditions, the amorphous CoO_xH_y structure remained largely unchanged but exhibited low OER activity. In contrast, in alkaline solution, the catalyst surface reorganized into a relatively ordered β-CoOOH layer, confirming that higher pH significantly promote structural reorganization. To probe the influence of temperature, Mai *et al.* examined the transformation of $NiMoO_4$ into NiOOH during the OER at varying electrolyte temperatures.[94] Their results revealed that elevated temperatures accelerate Mo leaching, thereby facilitating the formation of the NiOOH layer. As the temperature increased from 25 °C to 52 °C, the thickness of the reconstructed layer grew from ~6 nm to complete transformation.

(iii) Structure of precatalysts: the intrinsic structures of catalysts, such as crystal structure and chemical composition, play a decisive role in governing their reconstruction. In the case of iridate catalysts for acidic OER, the reconstructed phases are strongly influenced by their initial crystal structure. Chung *et al.* systematically classified eleven iridates into three categories based on the connectivity of IrO_6 octahedra:[95] (A) strongly edge-shared or face-shared IrO_6 networks, including $BaIrO_3$ and Ca_2IrO_4; (B) intermediate corner-shared IrO_6 frameworks, such as $SrIrO_3$, $CaIrO_3$, and $A_2Ir_2O_7$ (A = Y, Pr, Nd); and (C) weakly corner-shared or isolated IrO_6 units, exemplified by $Ba_4Ir_3O_{10}$, Sr_2IrO_4, Ca_4IrO_6, and Sr_4IrO_6. Post-OER surface and composition analyses revealed that the degree of IrO_6 connectivity critically determines structural robustness. Group A materials retained their octahedral framework even after A-site cation leaching, whereas Group C materials suffered rapid lattice collapse accompanied by dissolution of the IrO_6 network. Notably, even catalysts with identical bulk phase and composition can exhibit markedly different reconstruction behaviors, depending on the exposed crystal facets and crystallinity.[96–98]

Catalyst reconstruction is intrinsically governed by its electronic structure. For OER catalysts, parameters such as the oxygen p-band center and the metal d-band center have been proposed to correlate with the structural stability of metal oxides.[99–101] Recently, our group investigated a series of 66 $SrBO_3$ perovskite oxides (B = Ti, Ru, Ir) with varied Ti : Ru : Ir atomic ratios as acidic OER catalysts.[102] We demonstrated that the degree of hybridization between the mixed transition-metal d orbitals and oxygen 2p orbitals plays a pivotal role in determining stability. Excessively strong B–O covalency, as in $SrRuO_3$, facilitates the activation of lattice oxygen and the formation of amorphous IrO_x. In contrast, optimized B–O bond covalency, as observed in $SrTi_{0.2}Ru_{0.2}Ir_{0.6}O_3$, can effectively suppress surface reconstruction.

4. Regulation strategies of reconstruction

With the growing understanding of reconstruction, deliberate strategies have been developed to direct this process toward the formation of favorable active phases while suppressing detrimental transformations. Such control offers a pathway to the rational design of electrocatalysts that simultaneously achieve superior activity, enhanced stability, and high selectivity.

4.1 Structure design of pre-catalysts

Crystal phase engineering serves as an efficient strategy to regulate catalyst reconstruction. Among perovskite oxides, $SrIrO_3$ has attracted considerable attention as promising catalysts for acidic OER (Fig. 4a).[78,79,103] Under harsh acidic and oxidative environments, Sr cations are prone to leaching, which destabilizes the perovskite lattice and eventually leads to its collapse into amorphous IrO_x as the actual catalytically active phase (Fig. 4b and c). Reconstruction behaviors of these iridate catalysts in acidic OER represent typical examples of those shown in Fig. 2b and c. In our work, we selectively synthesized two distinct crystal phases of $SrIrO_3$, namely 6H-$SrIrO_3$ and 3C-$SrIrO_3$.[104] The 6H phase features both corner-sharing IrO_6 octahedra and face-sharing IrO_6 dimers, whereas the 3C phase exclusively consists of corner-sharing IrO_6 units. Compared with its 3C counterpart, the 6H phase effectively suppresses cation dissolution and structural reconstruction, thereby enhancing catalytic durability. More recently, we further developed an open-framework $SrIrO_3$ (Fig. 4d), which, unlike the 6H and 3C phases, undergoes an unusual crystalline-to-crystalline transformation during the OER,[80] yielding rutile-type IrO_2 nanocrystallites as the stable active phase. In addition, layered iridates such as honeycomb-like $SrIr_2O_6$, Na_2IrO_3, and Ruddlesden–Popper Sr_2IrO_4 have also been explored, demonstrating their potential to mitigate framework degradation and evade the conventional trade-off between OER activity and structural stability (Fig. 4e).[105–107] Consequently, the layered iridium oxide with well-designed nanostructures have been proven to deliver both high performance and durability in proton exchange membrane (PEM) water electrolyzers.[108,109]

Tuning the exposed crystal facets has emerged as an effective strategy to modulate reconstruction. Theoretical studies on $SrIrO_3$ revealed that its stability in acidic media strongly depends on the exposed crystal facet, with the (001) facet exhibiting greater resistance to Sr leaching compared to other orientations.[96] Guided by this result, 2D ultrathin (001)-faceted $SrIrO_3$ perovskites were synthesized. Unlike conventional $SrIrO_3$ particles, which undergo surface amorphization into a few-nanometer-thick IrO_x layer under acidic OER conditions, the (001)-faceted $SrIrO_3$ preserves high crystallinity in its surface region even after long-term operation. A similar facet-dependent behavior has also been observed in Ni-based OER catalysts. Zhu and co-workers uncovered a nanoscale surface restructuring process that preferentially occurs at the edge facets of β-$Ni(OH)_2$ during the OER, leading to the formation of Ni-deficient $Ni_{1-x}O$ enriched in Ni^{3+} species.[110] This transformation

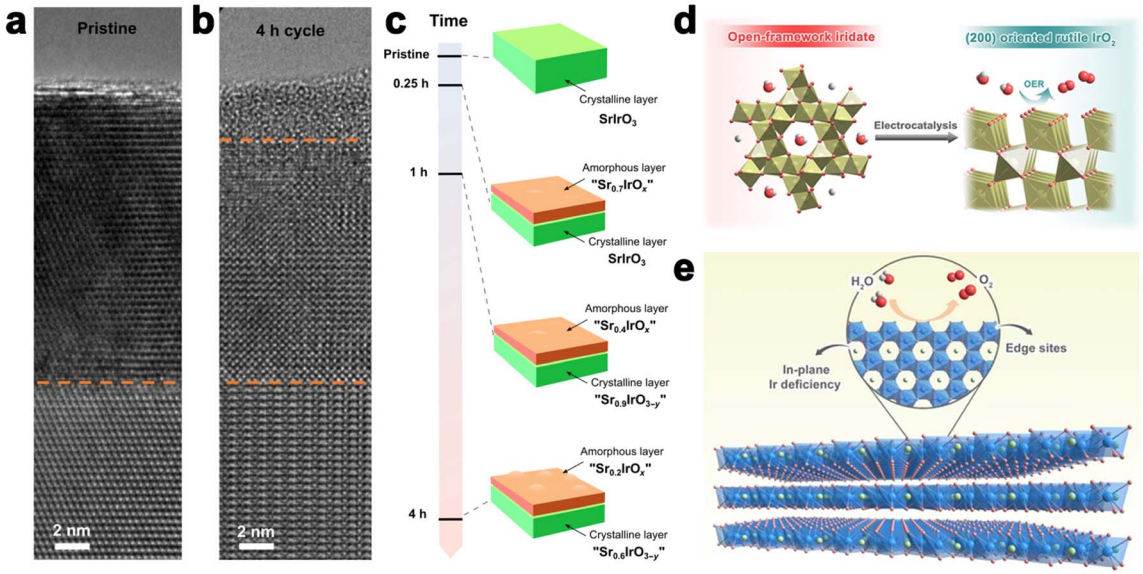

Fig. 4 (a and b) Cross-sectional TEM images of $SrIrO_3$ before and after 4 hours of potential cycling between 1.05 and 1.75 V *vs.* RHE. (c) Schematic illustration summarizing Sr leaching from the amorphous IrO_x layer throughout the amorphization process, accompanied by Sr concentration profiles. Reproduced with permission.[78] Copyright 2021, Springer Nature. (d) An open-framework iridate serves as a pre-electrocatalyst for the acidic OER, undergoing an atypical crystalline-to-crystalline transformation under reaction conditions. Reproduced with permission.[80] Copyright 2023, Wiley-VCH GmbH. (e) A layered iridate electrocatalyst exhibits high structural stability during the OER, maintained by its robust honeycomb-like layers consisting of edge-sharing IrO_6 octahedra. Reproduced with permission.[107] Copyright 2024, Wiley-VCH GmbH.

increases the density of exposed active sites and markedly enhances catalytic activity. Based on these findings, they further designed β-$Ni(OH)_2$ with enlarged edge facets, which, after surface reconstruction, outperformed even benchmark IrO_2 in OER performance.

Heteroatom doping provides an effective means of accelerating the reconstruction dynamics of electrocatalysts. For 3d transition-metal catalysts, the MOOH phase generally serves as the catalytically active state due to oxidation reconstruction (Fig. 2a), and cation doping has been shown to promote this transformation. For instance, Fe incorporation into Co_3O_4 facilitates its conversion into Fe–CoOOH during the OER,[111] while Cr-doped $NiFe_2O_4$ undergoes Cr leaching under CV activation,[112] thereby promoting the formation of NiFe oxyhydroxide and markedly enhancing catalytic performance. Similarly, Pt doping in Ni_2P promotes the generation of abundant high-valence NiOOH species,[113] where Pt sites redistribute the local charge density around Ni centers, and facilitate C–N bond cleavage, ultimately boosting the yield of value-added nitrite. In addition to cation doping, anion incorporation also proves effective in directing favorable reconstruction pathways. For example, Se-doped cobalt phosphide (Se-CoP) undergoes accelerated structural transformation,[114] yielding highly crystalline and robust $Co(OH)_2$/Co heterostructures that act as the true catalytic sites for synergistic HER. More recently, Zhang *et al.* introduced chlorine into $Bi_{19}Cl_3S_{27}$ nanowires, where the doped Cl atoms induce an intrinsic electric field.[115] The introduction of Cl accelerates the reconstruction kinetics, and creates vacancy defects, thereby achieving high activity and selectivity for CO_2-to-formate conversion.

Noble-metal catalysts are typically dispersed on supports to maximize metal utilization, and the choice of support can play a decisive role in governing reconstruction pathways. Conventional Ir-based catalysts often undergo surface amorphization into hydrous IrO_x species during acidic OER, which compromises their stability.[116] Recent studies, however, have revealed an alternative reconstruction route for supported Ir nanoparticles:[90] when anchored on a TiO_x@Ti substrate, Ir undergoes a bulk phase transition from metallic Ir to crystalline rutile IrO_2 under electrochemical conditions (Fig. 5a). Unlike the conventional surface-limited amorphization process, this support-induced crystallization promotes a mechanistic shift from lattice oxygen participation to a complete adsorbate evolution mechanism, as verified by both mechanistic and structural characterization studies. As a result, the Ir/TiO_x@Ti catalyst delivers not only enhanced OER activity but also outstanding durability in acidic environments, validated in PEM water electrolyzers. More recently, an alternative support strategy was proposed to suppress Ir dissolution during reconstruction (Fig. 5b).[117] In this case, TiN supports induce a leaching-driven Ti trapping effect that effectively stabilizes amorphous IrO_x formed under OER conditions. During operation, Ti atoms leach from the TiN substrate and partially oxidize, depositing as Ti–O species on IrO_x clusters. These species mitigate the overoxidation of Ir(III) centers, thereby preserving catalytic stability over long-term operation.

Beyond catalyst supports, introducing a secondary phase within catalysts can also influence their reconstruction behavior. The dynamic and complex nature of the CO_2RR makes it challenging to steer the reconstruction process toward

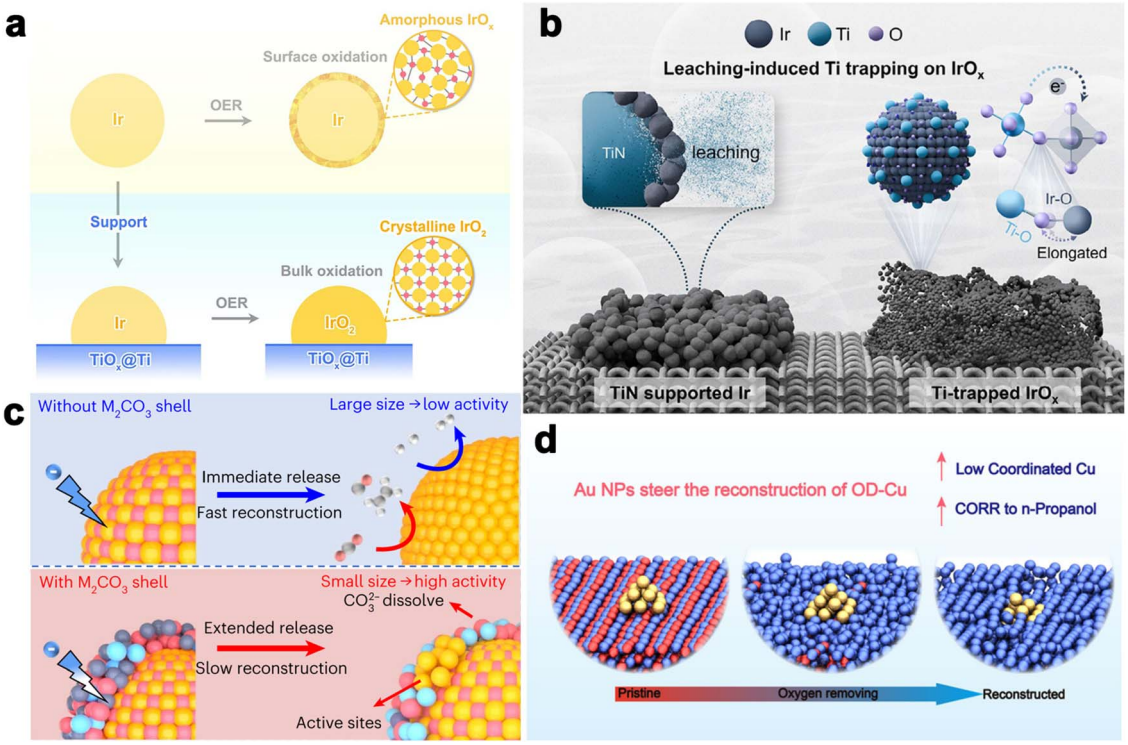

Fig. 5 (a) Schematic illustration of the electrochemically induced reconstruction process of Ir nanoparticles, contrasting scenarios with and without a TiO_x@Ti substrate. Reproduced with permission.[90] Copyright 2025, Springer Nature. (b) Schematic illustration of leaching of Ti from a TiN support contributes to a trapping mechanism that stabilizes amorphous IrO_x species during the OER. Reproduced with permission.[117] Copyright 2025, Wiley-VCH GmbH. (c) Comparative schematic depicting the projected structural reconstruction pathways of unmodified CuO and carbonate-coated CuO during electrochemical CO_2 reduction. Reproduced with permission.[118] Copyright 2025, Springer Nature. (d) Transformation of CuO into undercoordinated Cu sites localized near Au nanoparticles during CO electroreduction. Reproduced with permission.[119] Copyright 2024, American Chemical Society.

the formation of highly active and desirable surface structures. To address this issue, one innovative strategy involves the application of a water-soluble carbonate shell as a protective layer on metal oxide catalysts (Fig. 5c).[118] This coating effectively decelerates the surface reduction process, inhibiting the rapid transition of the catalyst from a high to a low valence state under an applied electric field. As a result, the controlled reconstruction promotes the formation of metallic Cu(0) species characterized by abundant grain boundaries and refined particle size, both of which are beneficial for enhancing catalytic performance. Cui and co-workers, for example, demonstrated that decorating Au nanoparticles on CuO nanosheets could steer the reconstruction of oxide-derived Cu (Fig. 5d).[119] Without Au decoration, surface Cu atoms tend to rearrange into ordered structures during electroreduction. In contrast, the presence of Au nanoparticles induces a more disordered Cu surface with a higher density of coordinatively unsaturated Cu atoms surrounding the Au sites, thereby enabling the selective electroreduction of CO into *n*-propanol.

Various chemical groups have been demonstrated to regulate the reconstruction behavior of electrocatalysts, such as sodium dodecyl sulfate (SDS), PO_4^{3-}, and MoO_4^{2-}.[120–123] In seawater electrolysis, designing catalysts that can withstand Cl^--induced corrosion while maintaining long-term stability is a central challenge. Yang and co-workers showed that the incorporation of phosphate (PO_4^{3-}) groups into Ni_3FeN accelerated its *in situ* surface reconstruction,[123] thereby generating a higher density of catalytically active species and simultaneously improving resistance against Cl^- attack. This dual effect highlights the potential of functional group engineering as an effective strategy to couple enhanced activity with corrosion tolerance in practical electrolysis systems.

4.2 Electrolyte engineering

Aqueous electrolytes typically contain a wide range of ionic species, including cations (*e.g.*, Mg^{2+}, Ca^{2+}, Cs^+, K^+, Na^+, and Li^+),[124–126] anions (*e.g.*, HCO_3^-, CO_3^{2-}, HPO_4^{2-}, ClO_4^-, SO_4^{2-}, F^-, Cl^-, Br^-, and I^-),[127] as well as small-molecule additives such as phosphate buffer saline (PBS), ethylenediamine tetramethylenephosphonic acid (EDTMPA), and *N*,*N*′-ethylene-phenanthrolinium dibromide.[128–130] These electrolyte components have been found to substantially influence catalytic activity and product selectivity. More recently, growing attention has been directed toward their role in governing the reconstruction of electrocatalysts. Understanding how electrolyte ions and additives modulate reconstruction pathways and determine the nature of reconstructed structures provides valuable guidance for rational catalyst design and performance optimization in CO_2 electroreduction.

Cu-based catalysts are prone to unavoidable and often uncontrollable surface reconstruction during electrocatalysis in the CO_2RR, which may either impair or enhance their performance. To address this challenge, Yang *et al.* proposed a strategy that directs the reconstruction pathway toward a favorable configuration using electrolyte additives.[129] Specifically, the introduction of EDTMPA enables controlled surface restructuring by selectively adsorbing on Cu(110) facets. This preferential adsorption not only promotes the selective exposure of Cu(110) surfaces with intrinsically strong *CO binding but also creates a local chemical environment that facilitates proton transfer from water to Cu(110), thereby enhancing catalytic efficiency. Electrolyte species can also drive reconstruction on oxide-derived catalysts. Deng *et al.* systematically investigated CO_3^{2-} adsorption on metal oxides and revealed its role in modulating structural evolution (Fig. 6a).[131] In the case of Bi_2O_3, which exhibits weak affinity toward CO_3^{2-}, the catalyst undergoes chemical transformation into a $Bi_2O_2CO_3/Bi_2O_3$ heterostructure under the carbonate-containing electrolyte. The *in situ* generated heterostructure acts as a highly active phase for formate production.

Beyond the CO_2RR, electrolyte-induced *in situ* surface reconstruction has also been observed in other electrocatalytic organic molecule transformation. Sun *et al.* reported that $CdPS_3$ nanosheets undergo electrolyte-triggered surface restructuring, which enables efficient electrochemical hydrogenation of 5-hydroxymethylfurfural (HMF) to 2,5-bis(hydroxymethyl)furan (BHMF) under ambient conditions (Fig. 6b).[130] In this system, the PBS electrolyte plays a pivotal role in driving the reconstruction, leading to the formation of a surface-bound CdS layer and the establishment of a $CdPS_3$/CdS heterostructure. This reconstructed material delivers remarkable catalytic performance, achieving a faradaic efficiency of 91% and a BHMF yield of 5 mg h^{-1} at −0.7 V. Together, these studies underscore the pivotal role of electrolyte additives and anions in steering reconstruction dynamics. These electrolyte-regulation strategies offer a new perspective for controlling the reconstruction of catalysts (Fig. 2d).

Despite these promising applications, a cautious approach is warranted. The introduction of electrolyte additives, such as F^- ions, can lead to unintended system-level consequences, including the degradation of proton exchange membranes.[132,133] Thus, advancing this strategy requires a balanced focus on both catalytic enhancement and the rigorous assessment of additive stability, crossover, and component compatibility under realistic operating conditions.

5. Characterization techniques for exploring reconstruction

Catalyst reconstruction under operational conditions represents a transformative process in electrocatalysis, wherein initially prepared phases evolve into metastable or even transient structures that mediate the reaction. Capturing these transformations requires *operando* techniques that probe both bulk crystallography and surface chemistry in real time (Fig. 7), which is indispensable for establishing casual links between evolving surface structures and catalytic activity. In this section, we first address the structural and spectroscopic methods for bulk and surface/interface characterization, followed by electrochemical-coupled analytical techniques that resolve transient reaction products.

5.1 Characterization of bulk and surface/interface structures

X-ray–based methodologies represent a cornerstone among *operando* tools for monitoring catalyst restructuring. In particular, *operando* XRD provides direct insights into crystallographic evolution by tracking changes in diffraction peaks that reflect lattice expansion, contraction, or the appearance of new

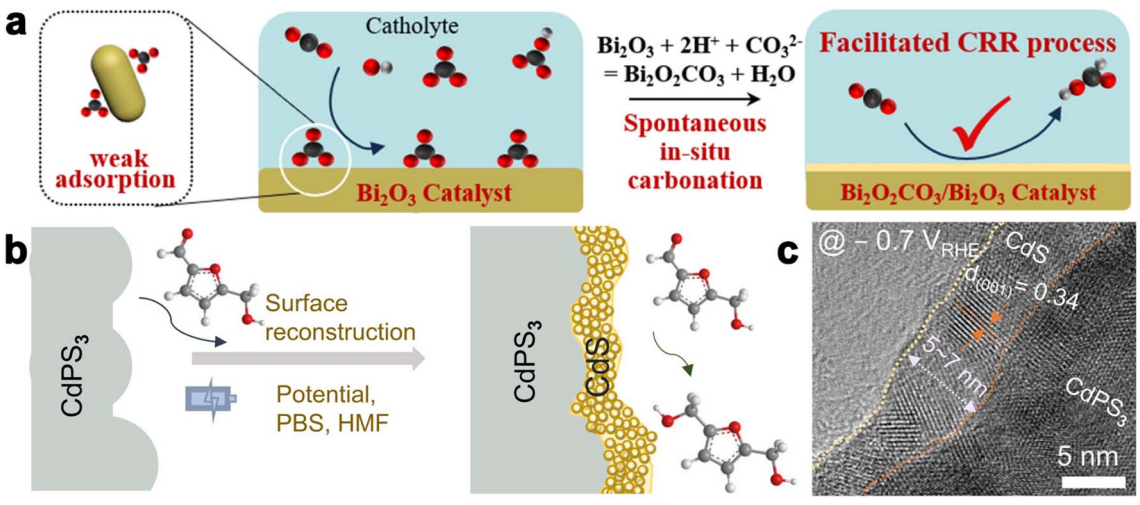

Fig. 6 (a) Schematic representation of the influence of CO_3^{2-} within the electrolyte microenvironment on the chemical evolution and electrocatalytic performance of metal oxides. Reproduced with permission.[131] Copyright 2024, Wiley-VCH GmbH. (b) Schematic illustration of the *in situ* surface reconstruction process of $CdPS_3$ during the hydrogenation of HMF. (c) Structural characterization of $CdPS_3$ after HMF hydrogenation. Reproduced with permission.[130] Copyright 2024, Springer Nature.

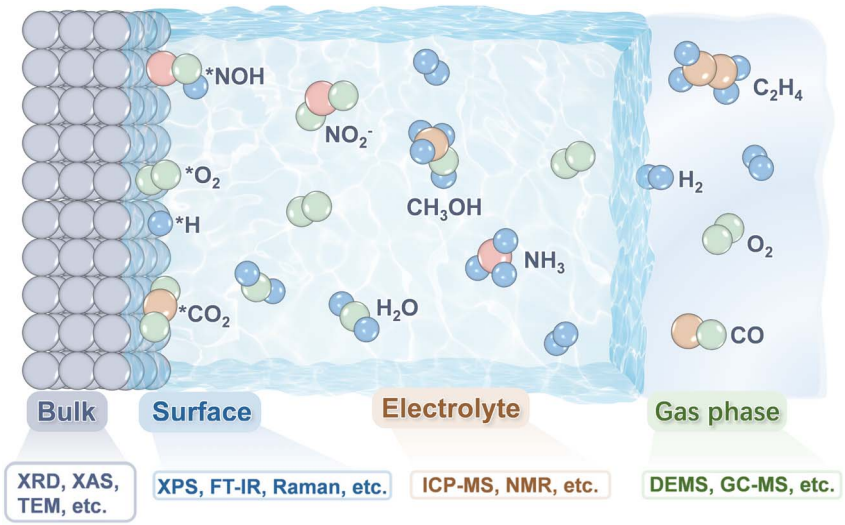

Fig. 7 Schematic overview of key characterization techniques for probing reconstruction processes, covering the catalyst bulk structure, the solid–liquid interface, the electrolyte microenvironment, and the gas-phase environment. XRD, XAS, TEM, XPS, FT-IR, ICP-MS, NMR, DEMS and GC-MS represent X-ray diffraction, X-ray absorption spectroscopy, transmission electron microscopy, X-ray photoelectron spectroscopy, Fourier transform infrared spectroscopy, inductively coupled plasma mass spectrometry, nuclear magnetic resonance, differential electrochemical mass spectrometry, and gas chromatography-mass spectrometry, respectively.

phases. For instance, Yan and co-workers reported that co-electrodeposition of Ni hydroxide with Ce oxide yields a $NiCeO_xH_y$ precursor.[134] Under anodic polarization, *operando* XRD revealed the formation of γ-NiOOH at relatively low overpotentials, accompanied by a distinctive exposure of the (003) facet, in contrast to conventional $Ni(OH)_2$ that preferentially exposes the (006) facet. This observation suggests that the enlarged lattice spacing in $NiCeO_xH_y$ enhances OER performance by facilitating hydroxide intercalation and exposing additional active sites. In a separate study, Yang *et al.* employed *operando* XRD to show that α-Li_2IrO_3 undergoes a phase transformation to α-$LiIrO_3$ during electrochemical cycling in KOH.[135] This transition was marked by a pronounced shift of the (003) diffraction peak from 18.7° to 12.6°, triggered by the interaction between α-$LiIrO_3$ and intercalated K^+ ions, ultimately leading to improved OER activity. While *operando* XRD is particularly powerful for monitoring the bulk evolution of long-range ordered crystalline phases during catalysis, its applicability is limited when dealing with amorphous materials.

Beyond crystallography, the reconstruction of electrocatalysts is also dictated by local electronic and coordination changes. *Operando* X-ray absorption spectroscopy (XAS) offers a powerful means to track such transformations, providing real-time information on oxidation states, coordination environments, and bond distances under working conditions. Enman and co-workers employed *operando* XAS to monitor the valence evolution of cobalt species in $Co(Fe)O_xH_y$.[136] As the potential increased from 0.1 V to 0.4 V, the edge energy of CoO_xH_y shifted upward by approximately 0.5 eV, consistent with partial oxidation of Co^{3+} to Co^{4+}. In contrast, for Fe-containing $Co(Fe)O_xH_y$, no potential-dependent shift in the Co K-edge was observed, implying that cobalt oxidation was suppressed in the presence of iron. In another study, *operando* XAS revealed dynamic bond-length changes in np-Ir/NiFeO catalysts.[137] The Ir–O bond was found to shrink during the OER, suggesting that iridium persists in an atomically dispersed configuration throughout operation. Simultaneously, variations in the white line intensity indicated the generation of active oxygen species during the deprotonation step, a process identified as critical for accelerating OER kinetics.

Surface-sensitive spectroscopies provide indispensable insight into chemical and electronic dynamics at the surface of catalysts. *Operando* ambient-pressure X-ray photoelectron spectroscopy (AP-XPS) enables direct probing of surface composition, elemental states, and electronic structures under reaction conditions. By following potential-dependent shifts in core-level binding energies, AP-XPS clarifies how metal cations undergo valence cycling during catalysis. For example, Lettenmeier *et al.* found that *operando* XPS measurements can monitor the evolution of iridium oxidation states during the OER.[138] With increasing applied potential, the relative contributions of metallic Ir, Ir^{3+}, and Ir^{4+} species gradually shift, with Ir^{3+} being oxidized to Ir^{4+}. Consequently, the near-surface iridium nanoparticles were found to be predominantly presented in the Ir^{4+} state.

In parallel, vibrational spectroscopies such as *operando* Raman and infrared spectroscopy provide molecular-level fingerprints of surface transformations. These techniques are particularly powerful for detecting adsorbed intermediates, thereby elucidating reaction pathways. Our group, for instance, monitored the Raman response of H_4IrO_4 during the OER and observed a red shift of Ir(IV)–OH vibrational peaks as the potential increased.[105] This spectral evolution was attributed to deprotonation at the catalyst surface, offering direct mechanistic evidence for the role of surface hydroxyl groups in OER kinetics. Infrared spectroscopy, which leverages the

characteristic vibrational fingerprints of chemical bonds, has likewise proven effective for probing surface adsorbates. We applied *operando* infrared spectroscopy to compare the OER behavior of porous IrO_x with that of rutile IrO_2. Remarkably, once the applied potential exceeded 1.3 V, a distinct *O–O* vibrational feature emerged in the porous IrO_x sample, associated with direct bond formation between neighboring Ir–O units.[109] This finding indicated that the porous IrO_x catalyst proceeds the OER with little involvement of the oxide path mechanism.

Direct visualization plays a decisive role in elucidating nanoscale reconstruction phenomena. *Operando* transmission electron microscopy (TEM) enables real-time monitoring of catalyst morphology, structural rearrangements, and compositional changes under electrochemical conditions. Ortiz Peña and co-workers employed *in situ* TEM to examine the behavior of Co_3O_4 during the OER.[139] Their study revealed that the nanoparticle surface underwent irreversible amorphization, giving rise to a nanometric cobalt (oxyhydr)oxide-like phase. In another investigation, Yao and colleagues utilized *operando* liquid TEM to probe the reconstruction of β-$Ni(OH)_2$.[110] When the applied potential reached 1.5 V, a contraction in lattice spacing was detected, accompanied by transformation into the β-NiOOH phase. This structural reorganization enhanced the exposure of active sites and accelerated nickel oxidation kinetics, thereby promoting OER performance.

5.2 Electrochemical-coupled analytical techniques

Structural reconstruction is frequently accompanied by the dissolution of constituent elements, which can significantly influence both catalyst stability and the composition of products. Electrochemical-coupled analytical techniques provide a powerful bridge between material transformation and electrochemical response. Among these, online inductively coupled plasma mass spectrometry (ICP-MS) enables real-time quantification of metal dissolution during operation. Geiger and co-workers integrated a scanning flow cell with ICP-MS to continuously monitor the leaching behavior of various iridium-based perovskites under OER conditions.[103] Their results demonstrated that the preferential dissolution of non-noble elements promoted the formation of highly active amorphous iridium oxides, whereas the reconstructed Ir species themselves exhibited pronounced dissolution during oxygen evolution. Importantly, by correlating the dissolved Ir with the evolved oxygen, this study introduced the stability number (*S*-number) as a general metric to benchmark electrocatalyst durability.

In situ differential electrochemical mass spectrometry (DEMS) is a versatile *operando* technique for monitoring gaseous products during electrocatalysis. By integrating an electrochemical cell with a mass spectrometer, DEMS enables real-time detection and quantification of evolving species. This method is particularly valuable for oxygen evolution studies, where the use of isotope-labeled electrocatalysts allows DEMS to determine the origin of oxygen atoms in the generated O_2. For example, Wang and co-workers investigated iridium oxide nanosheets and rutile IrO_2 using ^{18}O labeling, and *operando* DEMS was employed to analyze the ratios of $^{34}O_2$ ($^{18}O^{16}O$) and $^{32}O_2$ ($^{16}O^{16}O$) during the OER.[107] Their results revealed a relatively higher fraction of $^{34}O_2$ in the products of the nanosheet catalyst, indicating that oxygen atoms from structural hydroxyl groups were incorporated into the OER cycle.

Taken together, *operando* characterization techniques provide a multidimensional toolkit that correlates structural evolution, electronic reconfiguration, and catalytic behavior. Importantly, reconstruction is not a simple transformation from one static phase to another; rather, it is a continuous process involving dissolution–reprecipitation, surface oxidation, and lattice rearrangement. By integrating complementary approaches, researchers can resolve the dynamic pathways through which pre-catalysts transform into their active states.

6. Conclusions and outlook

Surface reconstruction has emerged as a pivotal concept in understanding and regulating electrocatalysis. Unlike conventional *ex situ* synthesis strategies, *in situ* reconstruction can generate catalytically active sites that are otherwise inaccessible, thereby offering new opportunities for enhancing activity and stability. Nevertheless, this dynamic nature also poses challenges: the predesigned active motifs may evolve or even vanish under operational conditions, complicating the rational design of catalysts. Looking ahead, several key directions deserve further attention.

(i) Investigating reconstruction in realistic electrochemical devices: most current studies on catalyst reconstruction have been carried out in model three-electrode systems. In contrast, investigations within practical electrolyzers remain scarce, despite the fact that industrial devices operate under far more demanding conditions, such as high voltages, large current densities (>1 A cm^{-2}), and continuous gas–liquid interactions.[123,140,141] The reconstruction behavior and its impact on catalytic performance in such environments could deviate substantially from those observed in laboratory setups. Moreover, electrolyzers are often regarded as "black boxes", making direct monitoring of dynamic surface transformations challenging. Therefore, advancing methodologies that can probe reconstruction pathways and establish structure–activity relationships under device-relevant conditions will be crucial for bridging the gap between fundamental studies and practical applications.

(ii) Advancing theoretical modelling of reconstruction: for decades, static catalyst models have served as the foundation of electrocatalysis theory, successfully interpreting many experimental results, particularly for relatively stable catalyst systems. However, the frequent observation of restructuring has challenged this paradigm, highlighting the need to account for dynamic catalyst–electrolyte interfaces.[142,143] Developing theoretical frameworks that incorporate free-energy landscapes of reconstruction pathways is essential for capturing the transient nature of active sites. Integration of *in situ*/*operando* characterization techniques with advanced simulations, such as density

functional theory, molecular dynamics, and machine learning, offers the potential to reveal atomic-level mechanisms and provide predictive power for catalyst design.

(iii) Expanding electrolyte engineering for controlled reconstruction: while significant progress has been made in correlating pre-catalyst structures with their reconstructed states, the role of the electrolyte microenvironment in governing reconstruction remains underexplored. Emerging evidence suggests that electrolyte properties, including ion composition, pH, small-molecule additives, and temperature, can profoundly influence the kinetics and thermodynamics of reconstruction, thereby reshaping catalytic architectures.[144,145] Systematic studies on electrolyte engineering will not only deepen mechanistic understanding but also provide a novel avenue for tailoring dynamic surface chemistry.

(iv) Unravelling the synergy between chemical and physical driving forces: reconstruction is often viewed predominantly as a chemically driven process; however, physical factors can play equally important roles. Gas bubble nucleation and detachment, electrolyte convection, and atom migration through Ostwald ripening and/or growth–dissolution cycles can all contribute to morphological and structural evolution.[146] These processes may induce cracks, catalyst detachment, or particle coarsening, ultimately influencing both activity and durability. Since chemical and physical driving forces frequently act in concert, it is imperative to consider their synergistic effects when designing robust catalysts.

In summary, the dynamic reconstruction of electrocatalysts is both an opportunity and a challenge. A deeper integration of device-level studies, dynamic theoretical models, electrolyte engineering, and coupled chemical–physical perspectives will be vital for translating reconstruction chemistry into practical strategies for high-performance, durable electrochemical energy technologies.

Author contributions

H. Chen wrote the manuscript. L. Wang and M. Na helped with the manuscript preparation and figure design. X. Zou revised and supervised the manuscript. All authors revised and finalized the manuscript.

Conflicts of interest

There are no conflicts to declare.

Data availability

No primary research results, software or code have been included, and no new data were generated or analysed as part of this review.

Acknowledgements

X. Zou and H. Chen thank the National Natural Science Foundation of China (grant nos. 22179046 and 22279040), the Jilin Province Science and Technology Development Plan (grant no. 20240402080GH), and the Fundamental Research Funds for the Central Universities for their financial support.

References

1 T. Tang, X. Bai, Z. Wang and J. Guan, *Chem. Sci.*, 2024, **15**, 5082–5112.
2 H. Chen, X. Liang, Y. Liu, X. Ai, T. Asefa and X. Zou, *Adv. Mater.*, 2020, **32**, 2002435.
3 S. Zhao, Y. Yang and Z. Tang, *Angew. Chem., Int. Ed.*, 2022, **61**, e202110186.
4 T. Wang, X. Cao and L. Jiao, *Angew. Chem., Int. Ed.*, 2022, **61**, e202213328.
5 L. Xiao, Z. Wang and J. Guan, *Chem. Sci.*, 2023, **14**, 12850–12868.
6 F. Zhang, Y. Zhu, Q. Lin, L. Zhang, X. Zhang and H. Wang, *Energy Environ. Sci.*, 2021, **14**, 2954–3009.
7 R. Zhang, Y. Zhang, B. Xiao, S. Zhang, Y. Wang, H. Cui, C. Li, Y. Hou, Y. Guo, T. Yang, J. Fan and C. Zhi, *Angew. Chem., Int. Ed.*, 2024, **63**, e202407589.
8 H.-F. Zhao, L. Li, T. Zhang, J.-Q. Yao, X. Peng, J. Peng, M. Zhu, B.-B. Xu, X.-W. Liu and H.-B. Yu, *Sci. Adv.*, 2025, **11**, eadx6121.
9 M.-C. Zhang, Q.-Q. Liu, W.-P. Sun, K. Sun, Y.-C. Shen, W. An, L. Zhang, H. Chen and X.-X. Zou, *Chem. Synth.*, 2023, **3**, 28.
10 Y. Li, Z. Zhang, Y. Yang, C. Li, Z. Shi and S. Feng, *ACS Catal.*, 2025, **15**, 8361–8389.
11 Y. Wang, L. Wang, K. Zhang, J. Xu, Q. Wu, Z. Xie, W. An, X. Liang and X. Zou, *Chinese J. Catal.*, 2023, **50**, 109–125.
12 M. Zhang, X. Ai, X. Liang, H. Chen and X. Zou, *Adv. Funct. Mater.*, 2023, **33**, 2306358.
13 X. Bai, M. Zhang, Y. Shen, X. Liang, W. Jiao, R. He, Y. Zou, H. Chen and X. Zou, *Adv. Funct. Mater.*, 2024, **34**, 2400979.
14 Y. Jia and X. Yao, *Acc. Chem. Res.*, 2023, **56**, 948–958.
15 K. Li, Y. Kuwahara and H. Yamashita, *Chem. Sci.*, 2024, **15**, 854–878.
16 E. K. Volk, M. E. Kreider, D. M. Gibson Colón, M. Müller, S. Sunde, S. M. Alia and S. Kwon, *ACS Catal.*, 2025, **15**, 11475–11486.
17 X. Wang, H. Hu, J. Song, J. Ma, H. Du, J. J. Wang, M. Wang, W. Chen, Y. Zhou, J. Wang, M. Yang and L. Zhang, *Adv. Energy Mater.*, 2025, **15**, 2402883.
18 Q. Gong, P. Ding, M. Xu, X. Zhu, M. Wang, J. Deng, Q. Ma, N. Han, Y. Zhu, J. Lu, Z. Feng, Y. Li, W. Zhou and Y. Li, *Nat. Commun.*, 2019, **10**, 2807.
19 N. B. D. Monti, T. Chen, L. Huang, J. Wang, M. Fontana, C. F. Pirri, W. Ju and J. Zeng, *J. Phys. Chem. Lett.*, 2025, **16**, 3761–3768.
20 Z. Weng, Y. Wu, M. Wang, J. Jiang, K. Yang, S. Huo, X.-F. Wang, Q. Ma, G. W. Brudvig, V. S. Batista, Y. Liang, Z. Feng and H. Wang, *Nat. Commun.*, 2018, **9**, 415.
21 C. M. Gunathunge, X. Li, J. Li, R. P. Hicks, V. J. Ovalle and M. M. Waegele, *J. Phys. Chem. C*, 2017, **121**, 12337–12344.
22 L. Gao, X. Cui, C. D. Sewell, J. Li and Z. Lin, *Chem. Soc. Rev.*, 2021, **50**, 8428–8469.
23 J. Liu and L. Guo, *Matter*, 2021, **4**, 2850–2873.
24 G. Suresh and J. H. Bang, *Energy Fuels*, 2025, **39**, 4669–4692.

25 S. S. A. Shah, T. Najam, M. S. Bashir, M. S. Javed, A.-U. Rahman, R. Luque and S.-J. Bao, *Small*, 2022, **18**, 2106279.
26 M. Ning, S. Wang, J. Wan, Z. Xi, Q. Chen, Y. Sun, H. Li, T. Ma and H. Jin, *Angew. Chem., Int. Ed.*, 2024, **63**, e202415794.
27 L. Wang, Q. Pan, X. Liang and X. Zou, *ChemSusChem*, 2025, **18**, e202401220.
28 S. Chen, F. Farzinpour and N. Kornienko, *Chem*, 2025, **11**, 102575.
29 J.-W. Zhao, Y. Li, D. Luan and X. W. Lou, *Sci. Adv.*, 2024, **10**, eadq4696.
30 L. Wang, Q. Meng, M. Xiao, C. Liu, W. Xing and J. Zhu, *Renewables*, 2024, **2**, 272–296.
31 J. Li and J. Gong, *Energy Environ. Sci.*, 2020, **13**, 3748–3779.
32 X. Li, H.-Y. Wang, H. Yang, W. Cai, S. Liu and B. Liu, *Small Methods*, 2018, **2**, 1700395.
33 S. Chen, L. Ma, Z. Huang, G. Liang and C. Zhi, *Cell Rep. Phys. Sci.*, 2022, **3**, 100729.
34 H. Zhong, Q. Zhang, J. Yu, X. Zhang, C. Wu, Y. Ma, H. An, H. Wang, J. Zhang, X. Wang and J. Xue, *Adv. Energy Mater.*, 2023, **13**, 2301391.
35 S. Jin, *ACS Energy Lett.*, 2017, **2**, 1937–1938.
36 S. Xu, X. Ruan, M. Ganesan, J. Wu, S. K. Ravi and X. Cui, *Adv. Funct. Mater.*, 2024, **34**, 2313309.
37 R. Gao, M. Deng, Q. Yan, Z. Fang, L. Li, H. Shen and Z. Chen, *Small Methods*, 2021, **5**, 2100834.
38 R. Jena, V. Kashyap, R. Jana, T. Mandal, T. N. Das, F. A. Rahimi, S. Barman, D. Maity, R. Kumar, D. Bhattacharyya, A. Datta and T. K. Maji, *Angew. Chem., Int. Ed.*, 2025, **64**, e202510741.
39 D. Wu, L. Hu, X. Liu, T. Liu, X. Zhu, Q. Luo, H. Zhang, L. Cao, J. Yang, Z. Jiang and T. Yao, *Nat. Commun.*, 2025, **16**, 726.
40 X. Wang, Z. Peng, W. Zhou, X. Chen, Y. Tan, Y.-F. Huang, Z. Liu, W.-Q. Deng and H. Wu, *Angew. Chem., Int. Ed.*, 2025, **64**, e202504148.
41 K. Liu, H. Lan, Y. Chen, W. Tang, Z. Xiao, Y. Du, J. Xing, Z. Wu and L. Wang, *Chem. Sci.*, 2024, **15**, 19928–19935.
42 Y. Song, W. Zhao, Z. Wang, W. Shi, F. Zhang, Z. Wei, X. Cui, Y. Zhu, T. Wang, L. Sun and B. Zhang, *J. Am. Chem. Soc.*, 2025, **147**, 13775–13783.
43 J. Zhang, S. Xia, Y. Wang, J. Wu and Y. Wu, *iScience*, 2024, **27**, 110005.
44 C. Weng, Y. Song, K. Zou, Y.-X. Zhang, Z. Han, Y. Ma, H. Chen, X. Yang and W. Lin, *Adv. Energy Mater.*, 2025, **15**, 2502722.
45 W. Ma, S. Xie, X.-G. Zhang, F. Sun, J. Kang, Z. Jiang, Q. Zhang, D.-Y. Wu and Y. Wang, *Nat. Commun.*, 2019, **10**, 892.
46 R. M. Arán-Ais, F. Scholten, S. Kunze, R. Rizo and B. Roldan Cuenya, *Nat. Energy*, 2020, **5**, 317–325.
47 Z.-Z. Wu, F.-Y. Gao and M.-R. Gao, *Energy Environ. Sci.*, 2021, **14**, 1121–1139.
48 M. P. L. Kang, M. J. Kolb, F. Calle-Vallejo and B. S. Yeo, *Adv. Funct. Mater.*, 2022, **32**, 2111597.
49 C. Yang, S. Liang, C. Zhang, T. Zhang, W. Xie, M. Li and Q. Wang, *J. Energy Chem.*, 2025, **111**, 354–364.
50 Y. Liu, D. Tian, A. N. Biswas, Z. Xie, S. Hwang, J. H. Lee, H. Meng and J. G. Chen, *Angew. Chem., Int. Ed.*, 2020, **59**, 11345–11348.
51 H.-S. Bang, J. Jeon, J. Kang, Y.-J. Ko, C. Oh, H. Kim, X. Zhang, K. H. Choi, C. Woo, X. Dong, H. K. Yu, W. H. Lee, J.-Y. Choi and H.-S. Oh, *Small*, 2024, **20**, 2404343.
52 D. Cheng, K.-L. C. Nguyen, V. Sumaria, Z. Wei, Z. Zhang, W. Gee, Y. Li, C. G. Morales-Guio, M. Heyde, B. Roldan Cuenya, A. N. Alexandrova and P. Sautet, *Nat. Commun.*, 2025, **16**, 4064.
53 Y. Zhang, H. Liu, S. Zhao, C. Xie, Z. Huang and S. Wang, *Adv. Mater.*, 2023, **35**, 2209680.
54 Y. Zhong, Z. Sun, B. Y. Xia and Y. Su, *Chem. Eur. J.*, 2025, **31**, e202500770.
55 J. Feng, D. Shi, F. Wang, Y. Zou, W. Li, W. Zhang, H. Lin, Y. Meng and Q. Gao, *Chem. Sci.*, 2025, **16**, 12467–12475.
56 M. Yu, E. Budiyanto and H. Tüysüz, *Angew. Chem., Int. Ed.*, 2022, **61**, e202103824.
57 W. Li, D. Chen, Z. Lou, H. Yuan, X. Fu, H. Y. Lin, M. Lin, Y. Hou, H. Qi, P. F. Liu, H. G. Yang and H. Wang, *J. Am. Chem. Soc.*, 2025, **147**, 10446–10458.
58 J. Li, Y. Liu, H. Chen, Z. Zhang and X. Zou, *Adv. Funct. Mater.*, 2021, **31**, 2101820.
59 S. Li, Z. Li, R. Ma, C. Gao, L. Liu, L. Hu, J. Zhu, T. Sun, Y. Tang, D. Liu and J. Wang, *Angew. Chem., Int. Ed.*, 2021, **60**, 3773–3780.
60 C. Yang, Z. Dai, J. Yue, G. Wang and W. Luo, *Chem. Sci.*, 2025, **16**, 5266–5274.
61 R. Gao, G.-D. Li, J. Hu, Y. Wu, X. Lian, D. Wang and X. Zou, *Catal. Sci. Technol.*, 2016, **6**, 8268–8275.
62 L.-A. Stern, L. Feng, F. Song and X. Hu, *Energy Environ. Sci.*, 2015, **8**, 2347–2351.
63 S. Choi, S.-J. Kim, S. Han, J. Wang, J. Kim, B. Koo, A. A. Ryabin, S. Kunze, H. Hyun, J. Han, S.-C. Haw, K. H. Chae, C. H. Choi, H. Kim and J. Lim, *ACS Catal.*, 2024, **14**, 15096–15107.
64 C. Wu, X. Wang, Y. Tang, H. Zhong, X. Zhang, A. Zou, J. Zhu, C. Diao, S. Xi, J. Xue and J. Wu, *Angew. Chem., Int. Ed.*, 2023, **62**, e202218599.
65 A. Pedersen, K. Kumar, Y.-P. Ku, V. Martin, L. Dubau, K. T. Santos, J. Barrio, V. A. Saveleva, P. Glatzel, V. K. Paidi, X. Li, A. Hutzler, M.-M. Titirici, A. Bonnefont, S. Cherevko, I. E. L. Stephens and F. Maillard, *Energy Environ. Sci.*, 2024, **17**, 6323–6337.
66 J. Xu, C.-C. Kao, H. Shen, H. Liu, Y. Zheng and S.-Z. Qiao, *Angew. Chem., Int. Ed.*, 2025, **64**, e202420615.
67 T. Zhou, Y. Jing, Y. Yang, F. Yang, X. Yi and W. Sun, *Small*, 2025, **21**, 2409374.
68 J. Vavra, T.-H. Shen, D. Stoian, V. Tileli and R. Buonsanti, *Angew. Chem., Int. Ed.*, 2021, **60**, 1347–1354.
69 R. Zhang, N. Dubouis, M. Ben Osman, W. Yin, M. T. Sougrati, D. A. D. Corte, D. Giaume and A. Grimaud, *Angew. Chem., Int. Ed.*, 2019, **58**, 4571–4575.
70 Y. Jia, Y. Ding, T. Song, Y. Xu, Y. Li, L. Duan, F. Li, L. Sun and K. Fan, *Adv. Sci.*, 2023, **10**, 2303726.

71 F. Dionigi, Z. Zeng, I. Sinev, T. Merzdorf, S. Deshpande, M. B. Lopez, S. Kunze, I. Zegkinoglou, H. Sarodnik, D. Fan, A. Bergmann, J. Drnec, J. F. d. Araujo, M. Gliech, D. Teschner, J. Zhu, W.-X. Li, J. Greeley, B. R. Cuenya and P. Strasser, *Nat. Commun.*, 2020, **11**, 2522.
72 G. Wang, J. Liu, Y. Sui, M. Wang, L. Qiao, F. Du and B. Zou, *J. Mater. Chem. A*, 2019, **7**, 14876–14881.
73 D. Gao, H. Zhou, F. Cai, D. Wang, Y. Hu, B. Jiang, W.-B. Cai, X. Chen, R. Si, F. Yang, S. Miao, J. Wang, G. Wang and X. Bao, *Nano Res.*, 2017, **10**, 2181–2191.
74 Q. Zhang, H. Chen, L. Yang, X. Liang, L. Shi, Q. Feng, Y. Zou, G.-D. Li and X. Zou, *Chinese J. Catal.*, 2022, **43**, 885–893.
75 J.-W. Zhao, K. Yue, H. Zhang, S.-Y. Wei, J. Zhu, D. Wang, J. Chen, V. Y. Fominski and G.-R. Li, *Nat. Commun.*, 2024, **15**, 2928.
76 Y. Sim, T. G. Yun, K. H. Park, D. Kim, H. B. Bae and S.-Y. Chung, *Nat. Commun.*, 2025, **16**, 4152.
77 B. Lu, C. Wahl, R. dos Reis, J. Edgington, X. K. Lu, R. Li, M. E. Sweers, B. Ruggiero, G. T. K. K. Gunasooriya, V. Dravid and L. C. Seitz, *Nat. Catal.*, 2024, **7**, 868–877.
78 G. Wan, J. W. Freeland, J. Kloppenburg, G. Petretto, J. N. Nelson, D.-Y. Kuo, C.-J. Sun, J. Wen, J. T. Diulus, G. S. Herman, Y. Dong, R. Kou, J. Sun, S. Chen, K. M. Shen, D. G. Schlom, G.-M. Rignanese, G. Hautier, D. D. Fong, Z. Feng, H. Zhou and J. Suntivich, *Sci. Adv.*, 2021, **7**, eabc7323.
79 L. C. Seitz, C. F. Dickens, K. Nishio, Y. Hikita, J. Montoya, A. Doyle, C. Kirk, A. Vojvodic, H. Y. Hwang, J. K. Norskov and T. F. Jaramillo, *Science*, 2016, **353**, 1011–1014.
80 L. Yang, L. Shi, H. Chen, X. Liang, B. Tian, K. Zhang, Y. Zou and X. Zou, *Adv. Mater.*, 2023, **35**, 2208539.
81 L. Gu, Y. Cong, Z. Wu, F. Xie, Y. Hua, H. Xu and J. Yang, *Adv. Funct. Mater.*, 2025, 2500316.
82 H. Liao, T. Luo, P. Tan, K. Chen, L. Lu, Y. Liu, M. Liu and J. Pan, *Adv. Funct. Mater.*, 2021, **31**, 2102772.
83 C. W. Song, H. Suh, J. Bak, H. B. Bae and S.-Y. Chung, *Chem*, 2019, **5**, 3243–3259.
84 F. Guo, Y. Wu, H. Chen, Y. Liu, L. Yang, X. Ai and X. Zou, *Energy Environ. Sci.*, 2019, **12**, 684–692.
85 H. Zhang, W. Zhou, J. Dong, X. F. Lu and X. W. Lou, *Energy Environ. Sci.*, 2019, **12**, 3348–3355.
86 J.-W. DuanMu, Z.-Z. Wu, F.-Y. Gao, P.-P. Yang, Z.-Z. Niu, Y.-C. Zhang, L.-P. Chi and M.-R. Gao, *Precis. Chem.*, 2024, **2**, 151–160.
87 Z. Li, Z. Xie, H. Chen, X. Liang, X. Ai, L. Yuan, X. Li and X. Zou, *Chem. Eng. J.*, 2021, **419**, 129568.
88 S. Kunze, P. Grosse, M. Bernal Lopez, I. Sinev, I. Zegkinoglou, H. Mistry, J. Timoshenko, M. Y. Hu, J. Zhao, E. E. Alp, S. W. Chee and B. Roldan Cuenya, *Angew. Chem., Int. Ed.*, 2020, **59**, 22667–22674.
89 W. Ko, J. Shim, H. Ahn, H. J. Kwon, K. Lee, Y. Jung, W. H. Antink, C. W. Lee, S. Heo, S. Lee, J. Jang, J. Kim, H. S. Lee, S.-P. Cho, B.-H. Lee, M. Kim, Y.-E. Sung and T. Hyeon, *J. Am. Chem. Soc.*, 2025, **147**, 2369–2379.
90 K. Zhang, X. Liang, Y. Wang, Y. Zou, X. Zhao, H. Chen and X. Zou, *Nat. Commun.*, 2025, **16**, 8164.
91 A. Dutta, A. Kuzume, M. Rahaman, S. Vesztergom and P. Broekmann, *ACS Catal.*, 2015, **5**, 7498–7502.
92 A. Li, H. Ooka, N. Bonnet, T. Hayashi, Y. Sun, Q. Jiang, C. Li, H. Han and R. Nakamura, *Angew. Chem., Int. Ed.*, 2019, **58**, 5054–5058.
93 X. Duo, Z. Hu, H. Pan, B. Chen, F. Zhou, P. Liu, Y. Zhang, W. Luo, Z. Xie, R. Ouyang, X. Huang, J. Yu and Y. Wang, *J. Catal.*, 2025, **451**, 116355.
94 X. Liu, R. Guo, K. Ni, F. Xia, C. Niu, B. Wen, J. Meng, P. Wu, J. Wu, X. Wu and L. Mai, *Adv. Mater.*, 2020, **32**, 2001136.
95 C. W. Song, J. Lim, H. B. Bae and S.-Y. Chung, *Energy Environ. Sci.*, 2020, **13**, 4178–4188.
96 L. Yang, K. Zhang, H. Chen, L. Shi, X. Liang, X. Wang, Y. Liu, Q. Feng, M. Liu and X. Zou, *J. Energy Chem.*, 2022, **66**, 619–627.
97 W. Ding, D. Ji, K. Wang, Y. Li, Q. Luo, R. Wang, L. Li, X. Qin and S. Peng, *Angew. Chem., Int. Ed.*, 2025, **64**, e202418640.
98 Y. Zhao, X. Tan, W. Yang, C. Jia, X. Chen, W. Ren, S. C. Smith and C. Zhao, *Angew. Chem., Int. Ed.*, 2020, **59**, 21493–21498.
99 Z.-Q. Chen, W.-J. Cai, H.-J. Zhang, K. Xiao, B. Huang and Z.-Q. Liu, *Chem. Sci.*, 2025, **16**, 14750–14759.
100 Q. Zhang, X. Liang, H. Chen, W. Yan, L. Shi, Y. Liu, J. Li and X. Zou, *Chem. Mater.*, 2020, **32**, 3904–3910.
101 A. Grimaud, K. J. May, C. E. Carlton, Y.-L. Lee, M. Risch, W. T. Hong, J. Zhou and Y. Shao-Horn, *Nat. Commun.*, 2013, **4**, 2439.
102 X. Liang, W. Yan, Y. Yu, K. Zhang, W. An, H. Chen, Y. Zou, X. Zhao and X. Zou, *Angew. Chem., Int. Ed.*, 2023, **62**, e202311606.
103 S. Geiger, O. Kasian, M. Ledendecker, E. Pizzutilo, A. M. Mingers, W. T. Fu, O. Diaz-Morales, Z. Li, T. Oellers, L. Fruchter, A. Ludwig, K. J. J. Mayrhofer, M. T. M. Koper and S. Cherevko, *Nat. Catal.*, 2018, **1**, 508–515.
104 L. Yang, G. Yu, X. Ai, W. Yan, H. Duan, W. Chen, X. Li, T. Wang, C. Zhang, X. Huang, J.-S. Chen and X. Zou, *Nat. Commun.*, 2018, **9**, 5236.
105 H. Chen, L. Shi, K. Sun, K. Zhang, Q. Liu, J. Ge, X. Liang, B. Tian, Y. Huang, Z. Shi, Z. Wang, W. Zhang, M. Liu and X. Zou, *ACS Catal.*, 2022, **12**, 8658–8666.
106 L. Wang, L. Shi, Q. Liu, Y. Huang, W. Yan, X. Liang, X. Zhao, H. Chen and X. Zou, *ACS Catal.*, 2023, **13**, 7322–7330.
107 L. Wang, R. Du, X. Liang, Y. Zou, X. Zhao, H. Chen and X. Zou, *Adv. Mater.*, 2024, **36**, 2312608.
108 Z. Xie, X. Liang, Z. Kang, Y. Zou, X. Wang, A. Wu Yimin, G. King, Q. Liu, Y. Huang, X. Zhao, H. Chen and X. Zou, *CCS Chem.*, 2025, **7**, 216–228.
109 Z. Xie, H. Chen, X. Wang, Y. A. Wu, Z. Wang, S. Jana, Y. Zou, X. Zhao, X. Liang and X. Zou, *Angew. Chem., Int. Ed.*, 2025, **64**, e202415032.
110 Y. Yao, G. Zhao, X. Guo, P. Xiong, Z. Xu, L. Zhang, C. Chen, C. Xu, T.-S. Wu, Y.-L. Soo, Z. Cui, M. M.-J. Li and Y. Zhu, *J. Am. Chem. Soc.*, 2024, **146**, 15219–15229.
111 P. Guo, D. Liu, Q. Wang, P. Chen, H. Yang, M. Zhang, C. Zheng, L. Jiang, H. Pan and R. Wu, *Nano Lett.*, 2025, **25**, 10209–10217.

112 S. Luo, C. Dai, Y. Ye, Q. Wu, J. Wang, X. Li, S. Xi and Z. J. Xu, *Angew. Chem., Int. Ed.*, 2024, **63**, e202402184.
113 J. Zhang, J. Feng, J. Zhu, L. Kang, L. Liu, F. Guo, J. Li, K. Li, J. Chen, W. Zong, M. Liu, R. Chen, I. P. Parkin, L. Mai and G. He, *Angew. Chem., Int. Ed.*, 2024, **63**, e202407038.
114 X.-H. Zhang, M.-T. Zhang, H.-G. Du, H.-H. Huang, X.-F. Zhang, X. Wen, L.-D. Wang, W.-Z. Deng, Y.-M. He, J. Bai, L.-W. Ding and C.-T. He, *Angew. Chem., Int. Ed.*, 2025, **64**, e202507040.
115 X. Wang, Y. Zhang, S. Wang, Y. Li, Y. Feng, Z. Dai, Y. Chen, X. Meng, J. Xia and G. Zhang, *Angew. Chem., Int. Ed.*, 2024, **63**, e202407665.
116 W. Feng, B. Chang, Y. Ren, D. Kong, H. B. Tao, L. Zhi, M. A. Khan, R. Aleisa, M. Rueping and H. Zhang, *Adv. Mater.*, 2025, **37**, 2416012.
117 H. Y. Lin, W. J. Li, M. Y. Lin, H. G. Xu, S. R. Fang, Y. Lv, W. Li, J. Guo, H. Q. Fu, H. Y. Yuan, C. Sun, S. Dai, P. F. Liu and H. G. Yang, *Angew. Chem., Int. Ed.*, 2025, **64**, e202504212.
118 X. Ma, T. Yang, D. He, X. Gao, W. Jiang, D. Li, Y. Sun, X. Lin, J. Xu, H. Wang, X. Tai, Y. Lin, T. Yao, H. Zhou and Y. Wu, *Nat. Synth.*, 2025, **4**, 53–66.
119 C. Long, K. Wan, Y. Chen, L. Li, Y. Jiang, C. Yang, Q. Wu, G. Wu, P. Xu, J. Li, X. Shi, Z. Tang and C. Cui, *J. Am. Chem. Soc.*, 2024, **146**, 4632–4641.
120 Y. Lin, D. Huang, Q. Wen, R. Yang, B. Chen, Y. Shen, Y. Liu, J. Fang, H. Li and T. Zhai, *Proc. Nat. Acad. Sci.*, 2024, **121**, e2407350121.
121 Z. Li, X. Li, H. Zhou, Y. Xu, S.-M. Xu, Y. Ren, Y. Yan, J. Yang, K. Ji, L. Li, M. Xu, M. Shao, X. Kong, X. Sun and H. Duan, *Nat. Commun.*, 2022, **13**, 5009.
122 Z. Li, M. Li, Y. Chen, X. Ye, M. Liu and L. Y. S. Lee, *Angew. Chem., Int. Ed.*, 2024, **63**, e202410396.
123 H. Hu, X. Wang, Z. Zhang, J. Liu, X. Yan, X. Wang, J. Wang, J. P. Attfield and M. Yang, *Adv. Mater.*, 2025, **37**, 2415421.
124 J. Gu, S. Liu, W. Ni, W. Ren, S. Haussener and X. Hu, *Nat. Catal.*, 2022, **5**, 268–276.
125 Q. Wu and Z. J. Xu, *Angew. Chem., Int. Ed.*, 2025, **64**, e202505022.
126 H. Khani, A. R. Puente Santiago and T. He, *Angew. Chem., Int. Ed.*, 2023, **62**, e202306103.
127 X. Lu, W. Tu, Y. Zhou and Z. Zou, *Adv. Energy Mater.*, 2023, **13**, 2300628.
128 A. Thevenon, A. Rosas-Hernández, J. C. Peters and T. Agapie, *Angew. Chem., Int. Ed.*, 2019, **58**, 16952–16958.
129 Z. Han, D. Han, Z. Chen, J. Gao, G. Jiang, X. Wang, S. Lyu, Y. Guo, C. Geng, L. Yin, Z. Weng and Q.-H. Yang, *Nat. Commun.*, 2022, **13**, 3158.
130 M. G. Sendeku, K. Harrath, F. T. Dajan, B. Wu, S. Hussain, N. Gao, X. Zhan, Y. Yang, Z. Wang, C. Chen, W. Liu, F. Wang, H. Duan and X. Sun, *Nat. Commun.*, 2024, **15**, 5174.
131 X. Ren, F. Liu, H. Wu, Q. Lu, J. Zhao, Y. Liu, J. Zhang, J. Mao, J. Wang, X. Han, Y. Deng and W. Hu, *Angew. Chem., Int. Ed.*, 2024, **63**, e202316640.
132 M. Chandesris, V. Médeau, N. Guillet, S. Chelghoum, D. Thoby and F. Fouda-Onana, *Int. J. Hydrogen Energy*, 2015, **40**, 1353–1366.
133 Z. Rui, K. Hua, Z. Dou, A. Tan, C. Zhang, X. Shi, R. Ding, X. Li, X. Duan, Y. Wu, Y. Zhang, X. Wang, J. Li and J. Liu, *J. Mater. Chem. A*, 2024, **12**, 9563–9573.
134 Z. Yan, H. Sun, X. Chen, H. Liu, Y. Zhao, H. Li, W. Xie, F. Cheng and J. Chen, *Nat. Commun.*, 2018, **9**, 2373.
135 C. Yang, G. Rousse, K. Louise Svane, P. E. Pearce, A. M. Abakumov, M. Deschamps, G. Cibin, A. V. Chadwick, D. A. Dalla Corte, H. Anton Hansen, T. Vegge, J.-M. Tarascon and A. Grimaud, *Nat. Commun.*, 2020, **11**, 1378.
136 L. J. Enman, M. B. Stevens, M. H. Dahan, M. R. Nellist, M. C. Toroker and S. W. Boettcher, *Angew. Chem., Int. Ed.*, 2018, **57**, 12840–12844.
137 K. Jiang, M. Luo, M. Peng, Y. Yu, Y.-R. Lu, T.-S. Chan, P. Liu, F. M. F. de Groot and Y. Tan, *Nat. Commun.*, 2020, **11**, 2701.
138 P. Lettenmeier, J. Majchel, L. Wang, V. A. Saveleva, S. Zafeiratos, E. R. Savinova, J. J. Gallet, F. Bournel, A. S. Gago and K. A. Friedrich, *Chem. Sci.*, 2018, **9**, 3570–3579.
139 N. Ortiz Peña, D. Ihiawakrim, M. Han, B. Lassalle-Kaiser, S. Carenco, C. Sanchez, C. Laberty-Robert, D. Portehault and O. Ersen, *ACS Nano*, 2019, **13**, 11372–11381.
140 Q.-B. Huang, X. Zhang, S.-W. Lin, Y.-P. Liu, X.-X. Zou and H. Chen, *Chem. Synth.*, 2025, **5**, 57.
141 H. Chen, M. Na and X. Zou, *CCS Chem.*, 2025, **0**, 1–16.
142 W. Dai, K. Wan, K. Pang, J. Guo, S. Liu, K. Wu, C. Tang, Y. Sun, X. Shi, Z. Tang, C. Long and F. Dong, *Chem*, 2025, **11**, 102345.
143 H. Li, Y. Jiao, K. Davey and S.-Z. Qiao, *Angew. Chem., Int. Ed.*, 2023, **62**, e202216383.
144 H. Zhou, W. Xi, P. Yang, H. Huang, J. Tian, M. Ratova and D. Wu, *J. Energy Chem.*, 2024, **99**, 201–222.
145 J.-J. Lv, R. Yin, L. Zhou, J. Li, R. Kikas, T. Xu, Z.-J. Wang, H. Jin, X. Wang and S. Wang, *Angew. Chem., Int. Ed.*, 2022, **61**, e202207252.
146 I. Kim, G.-B. Lee, S. Kim, H. D. Jung, J.-Y. Kim, T. Lee, H. Choi, J. Jo, G. Kang, S.-H. Oh, W. Kwon, D. Hong, H. G. Kim, Y. Lee, U. Kim, H. Kim, M. Kim, S. Back, J. Park, Y.-C. Joo and D.-H. Nam, *Nat. Catal.*, 2025, **8**, 697–713.